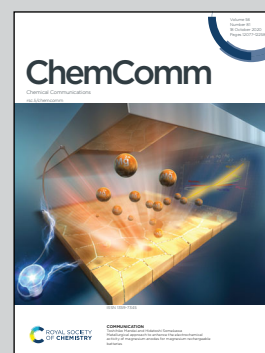


Showcasing research from Biophysics Laboratory/
Department of Physics and Inorganic Chemistry
Laboratory/Department of Chemistry,
School of Science, Kitasato University, Sagamihara,
Japan and Macromolecular Assembly Chemistry
Laboratory/Department of Molecular and
Macromolecular Chemistry, Graduate School of
Engineering, Nagoya University, Nagoya, Japan.

Visualizing the helical stacking of octahedral
metallomesogens with a chiral core

The stacking structure of a helical columnar liquid
crystal formed by enantiopure octahedral metallomesogens
with $\Delta\Lambda$ chirality was elucidated by a combination of
grazing-incidence X-ray diffraction, polarized optical
microscopy, and molecular dynamics simulation.

As featured in:



See Go Watanabe, Mitsuo Hara,
Jun Yoshida *et al.*,
Chem. Commun., 2020, **56**, 12134.



Visualizing the helical stacking of octahedral metallomesogens with a chiral core†

Cite this: *Chem. Commun.*, 2020, 56, 12134

Received 2nd September 2020,
Accepted 15th September 2020

DOI: 10.1039/d0cc05930g

rsc.li/chemcomm

A combination of grazing-incidence X-ray diffraction and molecular dynamics simulation studies led to the visualization of the stacking structure of a helical columnar liquid crystal formed by enantiopure octahedral metallomesogens with $\Delta\Lambda$ chirality. The helical structure was elucidated as a hybrid of two major proposed structures.

The introduction of chirality to liquid crystals (LCs) often leads to the spontaneous formation of macroscopic chiral structures.^{1,2} A nematic (N) LC, typically formed by achiral rod-shaped (calamitic) molecules, is well known to show a phase transition to a chiral nematic (N*) LC with a μm -scale helical pitch upon doping with chiral molecules.^{3,4} The introduction of chirality to columnar (Col) LCs mainly formed by discotic molecules^{5,6} can also induce macroscopic chiral structures, such as a helical stack of chiral mesogens.^{7–9} Helical Col LCs have attracted widespread research attention, for example, polar switching/ferroelectric materials, organic semiconductors with densely packed structures, and reaction fields for asymmetric reactions.^{10,11} In parallel, several stacking structures have been proposed for helical Col LCs; the major proposed structures are shown in Fig. 1 (types I, II, and III).¹⁰ Although the rational preparation of each helix type is necessary for the further development of helical Col LCs, it is currently challenging to even determine the helix type.¹² Molecular dynamics (MD) simulation based on detailed experimental data has been used as a powerful method to reveal the detailed structure of LCs. In fact, MD simulations for non-helical Col LCs have been actively performed in recent years.^{13,14} However, the

MD simulations with all-atom models have been applied to only helical Col LCs with type I structures, to the best of our knowledge.^{15–17}

A series of octahedral metallomesogens firstly reported by Giroud-Godquin and Rassat¹⁸ and later investigated in detail by Swager's group^{19,20} is unique and unconventional in the sense that they have propeller-shaped chirality at the molecular core ($\Delta\Lambda$ chirality). The effect of $\Delta\Lambda$ chirality on the resulting stacking structures was investigated indirectly; the introduction of enantiopure alkyl chains at the periphery of the octahedral mesogen resulted in the partial intercolumnar separation of the diastereomeric mixture.²⁰

Our research group has investigated chiral octahedral metal complexes, including enantiopure **Ru-C8** (Fig. 2a), as dopants for inducing N* phases, focusing on clarifying the relation between the molecular $\Delta\Lambda$ chirality and the resulting helical structures in N* phases.^{21–24} During the course of this study, we found that enantiopure **Ru-C8** aggregates in a nematic liquid crystal medium.²⁵ Here, we report the columnar liquid-crystalline

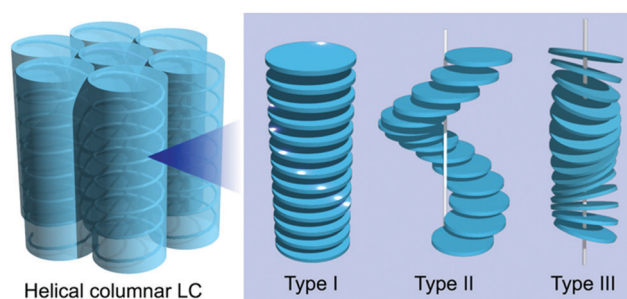


Fig. 1 Representative stacking structures proposed for helical Col LCs. The chiral parts, the center of the mass, and the normal vector of mesogens form helical structures in types I, II, and III, respectively. In type I, the chiral unit of each mesogen gradually rotates on the plane along the stacking direction, whereas, in type II, the positions of the mesogens translate on the plane to form a helix along the stacking direction. Mesogens can be either orthogonal or tilted relative to the column axis in types I and II.

^a Department of Physics, School of Science, Kitasato University, 1-15-1, Kitasato, Minami-ku, Sagami-hara 252-0373, Japan. E-mail: go0325@kitasato-u.ac.jp

^b Department of Chemistry, School of Science, Kitasato University, 1-15-1, Kitasato, Minami-ku, Sagami-hara 252-0373, Japan. E-mail: yoshidaj@kitasato-u.ac.jp

^c Department of Chemistry, Graduate School of Science and Engineering, Ehime University, 2-5, Bunkyo-cho, Matsuyama 790-8577, Japan

^d Department of Molecular and Macromolecular Chemistry, Graduate School of Engineering, Nagoya University, Furo-cho, Chikusa-ku, Nagoya, 464-8603, Japan. E-mail: mhara@chembio.nagoya-u.ac.jp

† Electronic supplementary information (ESI) available. See DOI: 10.1039/d0cc05930g

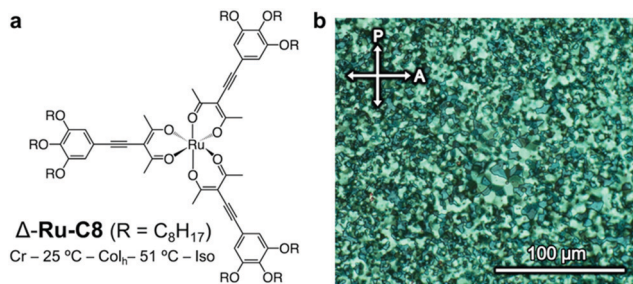


Fig. 2 (a) Molecular structure and phase behavior of the Δ isomer of **Ru-C8**. (b) Polarized optical micrographs of the textures displayed by Δ -**Ru-C8** in a Col_h phase at 40 °C (after annealing).

behaviour of enantiopure **Ru-C8** itself. Based on the X-ray diffraction (XRD) and molecular dynamics (MD) simulation studies, the helical stacking structure of enantiopure **Ru-C8** was elucidated as a hybrid of types II and III. The role of the core $\Delta\Lambda$ chirality in determining the resulting helical structure deduced from the analysis of the simulated structure will be discussed.

The phase behavior of Δ -**Ru-C8** was examined *via* differential scanning calorimetry (DSC, Fig. S4, ESI[†]), polarized optical microscopy (POM, Fig. 2b), and XRD. The mesophase observed in Δ -**Ru-C8** was identified as a hexagonal columnar (Col_h) phase. When Δ - or Λ -**Ru-C8** was cooled from the isotropic state to room temperature, it showed little indication of crystallization under POM observation. Their slow crystallization was confirmed by the time-course change of POM textures and XRD patterns (Fig. S5 and S6, ESI[†]). The details of the slow crystallization behavior are described in the ESI[†].

The XRD analysis of Δ -**Ru-C8** with a 1D detector reveals several diffraction peaks attributed to a Col_h phase with a lattice parameter of $a = 3.3$ nm (Fig. 3a), in addition to a broad diffraction corresponding to the alkyl halo and a peak at $d = 0.38$ nm (indicated by a red arrow in Fig. 3a), which is attributed to the repeat distance between adjacent mesogens, such as π - π stacking inside the columns. In contrast, a broad diffraction was observed around $2\theta = 3$ – 4° . To confirm the origin of this diffraction and obtain detailed structural information, GI-XRD analysis was conducted for the thin films of Δ - and Λ -**Ru-C8**, prepared by spin-coating their chloroform solutions on glass plates.

The GI-XRD image of Δ -**Ru-C8** taken at 37 °C shows spot-like reflections in the out-of-plane region (Fig. 3b). Since no surface treatment was performed on the glass plate, columns with planar and homeotropic alignments most likely co-existed on the glass plate. Indexing of most spots was possible by considering a reciprocal lattice of the Col_h phase with a planar alignment (green columns in the inset of Fig. 3b).^{26,27} The lattice parameter of the Col_h phase was deduced to be $a = 3.2$ nm, almost identical to that obtained from the 1D XRD analysis. In contrast, several reflections that are not on the grid points of the reciprocal lattice still remain: weak broad reflections highlighted by orange dotted arrows in Fig. 3b. The broad reflections periodically appear along the out-of-plane direction ($L = 1, 2, 3, \dots$ in Fig. 3b). Similar periodic reflections (layer-lines) were observed for helical Col LCs as the first- and higher-order

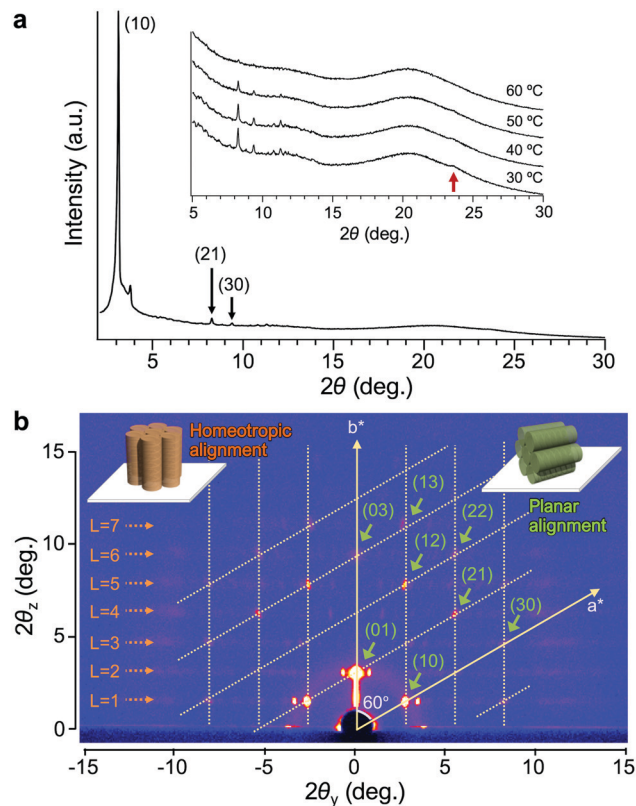


Fig. 3 (a) XRD patterns of Δ -**Ru-C8** obtained after annealing at 30 °C. The inset shows the VT-XRD patterns of Δ -**Ru-C8** in the wide angle region. The red arrow corresponds to the peak of $d = 0.38$ nm. (b) GI-XRD image of Δ -**Ru-C8** obtained at 37 °C. The reciprocal lattice of the Col_h phase with a planar alignment is overlaid. The periodic pattern attributed to the intracolumnar helix of homeotropically aligned columns is highlighted by dotted orange arrows. Schematic representations of columns with homeotropic and planar alignments are shown as insets in orange and green colors, respectively.

reflections based on the intracolumnar helix.^{28–31} The GI-XRD measurement of helical columns with a homeotropic alignment affords periodic broad reflections along the out-of-plane direction (orange columns in the inset of Fig. 3b). Based on the layer-lines, a helical pitch (p) was deduced to be 5.2 nm. Given the helical pitch ($p = 5.2$ nm) and the periodic distance between adjacent mesogens ($d = 0.38$ nm), a single pitch was deduced to comprise approx. 14 molecules. The simulated diffraction pattern based on these parameters matches fairly well with the experimental reflections (Fig. S7, ESI[†]). A similar diffraction pattern was also observed for the other enantiomer, Λ -**Ru-C8** (Fig. S8, ESI[†]).

To clarify the helical structure in enantiomeric **Ru-C8**, we then performed all-atom molecular dynamics (MD) simulations for Δ -**Ru-C8** based on the experimentally obtained structural information (approx. 14 molecules form a helical pitch of 5.2 nm) under periodic boundary conditions. As the initial structure, 16 columns with 2-fold helical pitches were positioned in the hexagonal lattice cell with dimensions of 12.95 nm \times 12.95 nm \times 10.60 nm. All the MD simulations were carried out using the program GROMACS 2016.6. The simulation details are provided

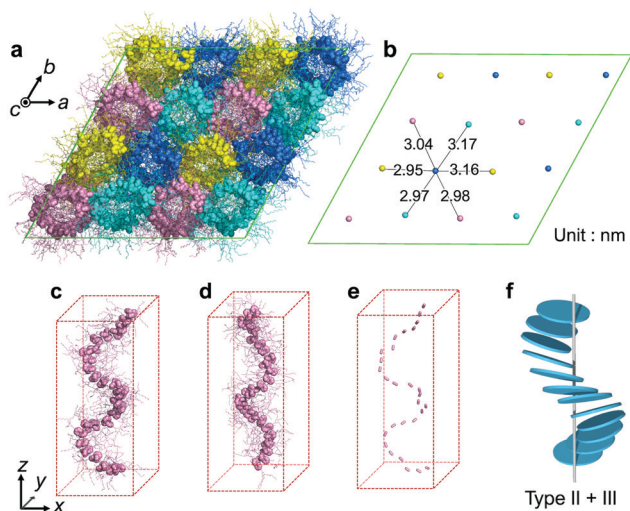


Fig. 4 (a) Top view of *M-Δ-Ru-C8* after 200 ns of MD simulation. The Ru core and peripheral groups in each mesogen molecule are represented by spheres and sticks, respectively. (b) Average positions of Ru atoms in each column. (c) Side view of a single column in *M-Δ-Ru-C8*. (d) Side view of a single column in *P-Λ-Ru-C8*. (e) The C_3 axis of each mesogen in (c) is displayed. (f) Schematic of a single-column structure in *M-Δ-Ru-C8*, corresponding to a hybrid of types II and III.

in the ESI†. In the initial structure, Δ -**Ru-C8** molecules were placed in a type I manner with the neighboring molecules rotated *ca.* 25° to each other, because the configurations without rotation resulted in an overlap of the ligands and the formation of undesirable void spaces between the columns. When 14 molecules were initially placed without tilting to form an *M* helical pitch, the calculations either did not reach the equilibrium state or resulted in structures without 2D periodicity. We then examined the initial configurations, in which 14 molecules were placed with the C_3 axis of each mesogen tilted approximately 5° from the column axis to form an *M* helical pitch. After the equilibration run at 310 K for 200 ns, the two-dimensional hexagonal packing of Δ -**Ru-C8** molecules was confirmed (Fig. 4a, b and Fig. S9–S14, ESI†). The helical stacking in a single column is shown in Fig. 4c, in which the neighboring atoms of ruthenium (Ru core) and other atoms are represented by spheres and stick models, respectively. The C_3 axes of each molecule in a single column are shown in Fig. 4e. The position and direction of each mesogen gradually rotate around the column axis, confirming the presence of a helical structure that is a hybrid of types II and III (Fig. 4f and Fig. S15, ESI†). The average lattice parameter of the hexagonal lattice obtained from the MD simulation was $a = 3.04 \pm 0.03$ nm, consistent with the experimentally obtained value ($a = 3.2$ nm by GI-XRD). The equilibrium structure with an *M* helix is hereafter denoted as *M-Δ-Ru-C8* (Fig. 4a and Fig. S16a, ESI†).

For comparison, we also examined the initial condition, under which 14 tilted Δ isomers were set to form an opposite *P* helix. After the equilibrated run at 310 K for 200 ns, deformed *P* helices were obtained (*P-Λ-Ru-C8*, Fig. S16b, ESI†). We then examined another initial condition, under which 14 tilted Λ -isomers were set to form a *P* helix (*P-Λ-Ru-C8*, Fig. 4d and Fig. S16c, S17, ESI†). The resulting helical structure was almost

antipodal to that of *M-Δ-Ru-C8*, indicating that Δ and Λ isomers favor the formation of *M* and *P* helices, respectively.

In *M-Δ-Ru-C8*, **Ru-C8** molecules with roughly Y-shaped molecular structures stack along the column axis, directing one ligand to the inner space of the helix, and spreading the other two ligands to the exterior of the helix. Three phenylene rings in each Δ -**Ru-C8** molecule are shown in Fig. 5a–c; they were positioned at the interior of the helix formed by the Ru core, close to the helix framework, and outside the helix. Intermittent π -stacking was observed between the phenylene rings positioned in the interior of the helix (Fig. 5a and Fig. S18a, ESI†), consistent with the XRD study (observation of the peak at $d = 0.38$ nm). In contrast, no π -stacking was observed between the other two phenylene rings (Fig. 5b and c). Similar stacking behavior is also observed in *P-Λ-Ru-C8* (Fig. S19, ESI†). When each **Ru-C8** molecule is viewed along the C_3 axis (at the center of the Y-shape), the three methyl groups protrude along the C_3 axis (Fig. S20a, ESI†), disturbing the efficient packing. To avoid steric repulsion, the Y-shaped molecules need to be slipped and twisted with each other, keeping the π -stacking (Fig. S18b and c, ESI†); the twisting direction (*M* or *P*) reflects the chiral structure of each mesogen, as shown in Fig. S16 (ESI†). The hybrid helical structure of types II and III is rational in terms of the π -stacking interaction and steric repulsion between chiral cores.

In addition to the molecular structure, we further consider the effect of dipolar interactions in the helix formation.^{32,33} The core structure of **Ru-C8**, [Ru(acacC₂Ph)₃], was deduced to have a dipole moment of *ca.* 0.92 Debye along the C_2 axis based on the DFT calculation (Fig. S20a, ESI†). Although [Ru(acacC₂Ph)₃] ideally has D_3 symmetry, it is slightly distorted and the paramagnetic spin is distributed to some extent over one of the three ligands.³⁴ Hence, [Ru(acacC₂Ph)₃] has a dipole moment along the C_2 axis. To examine the effect of dipolar interactions in *M-Δ-Ru-C8*, the dipole moments were then calculated for each **Ru-C8** molecule in a single column using the molecular coordinates obtained by MD simulations (Fig. S20b, c and S21, ESI†). The variable magnitudes of dipole moments are attributed to the fluctuation of the terminal alkyl chains. The distribution of dipole moments in a single column viewed along the side and top of the column highlights the balanced distribution of dipole moments in the xz and xy planes (Fig. S20c and S21, ESI†); the dipoles were cancelled within a helical pitch. The analysis of MD simulation results indicates that the interplay of steric repulsion, π - π interaction, and dipolar interaction is a driving force for enantiopure **Ru-C8** to form the helical structure.

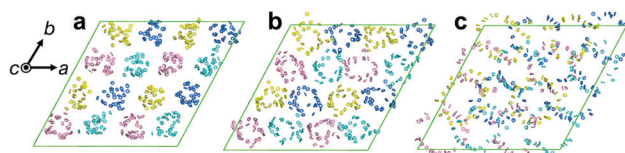


Fig. 5 Three phenylene groups in Δ -**Ru-C8** molecules are shown for *M-Δ-Ru-C8*: (a) those positioned at the interior of the helix, (b) those positioned near the Ru core, and (c) those positioned outside the helix.

In this paper, we mainly discussed the intermolecular interactions inside a column, which led to a helical assembly of octahedral metallomesogens; molecules stack with both the molecular position and the C_3 axis rotating along the column axis. In contrast, each resulting helical column, a hybrid of types II and III, is not a simple cylinder. Hence, helical columns need to assemble collectively to minimize the total energy of the system. The importance of efficient molecular packing has already been recognized for the cases of so-called star-shaped mesogens with three arms.^{35–37} Because star-shaped molecules have “free space” between the arms, their assembly structures are stabilized by filling the space with neighboring molecules or guests.³⁸ In our case, neighboring columns have similar helical manners to fill the “free space” (Movie S1, ESI†). The helical structure information appears to be transferred between neighboring columns, leading to the stabilization of the whole helical columnar assemblies as a hexagonal columnar phase.

In conclusion, the helical Col LC system was established using enantiopure octahedral metallomesogens with $\Delta\Lambda$ chirality at the molecular core (Δ - or Λ -Ru-C8). A combination of GI-XRD and MD simulation studies led to the visualization of the helical stacking structure as a hybrid of two major proposed structures, types II and III. Both type II and III structures have been proposed as basic structures for helical Col LCs, whereas the all-atom MD simulation of the hybrid structure is reported for the first time in this article, to the best of our knowledge. We believe that the revealed correlation between the core chiral mesogen and the helical stacking structure will lead to the rational development of helical Col LCs, including the control of stacking type.

We gratefully acknowledge Prof. Takahiro Ichikawa (Tokyo University of Agriculture and Technology) for his assistance in the XRD measurements and helpful discussions on this project. This work was financially supported by JSPS KAKENHI (Grant Numbers JP18K14283, JP19K05508, JP19H02537, JP19H05718, and JP20H05217). J. Y. and H. S. acknowledge the financial support from JST MIRAI (Grant Number JPMJMI18GC). G. W. and J. Y. acknowledge the financial support from Kitasato University Research Grant for Young Researchers. The computations were performed at the Research Center for Computational Science, Okazaki, Japan.

Conflicts of interest

There are no conflicts to declare.

Notes and references

- J. W. Goodby, M. A. Waugh, S. M. Stein, E. Chin, R. Pindak and J. S. Patel, *J. Am. Chem. Soc.*, 1989, **111**, 8119–8125.
- Chirality in Liquid Crystals*, ed. H.-S. Kitzerow and C. Bahr, Springer-Verlag, New York, 2001.
- G. Solladié and R. G. Zimmermann, *Angew. Chem., Int. Ed. Engl.*, 1984, **23**, 348–362.
- N. Katsonis, E. Lacaze and A. Ferrarini, *J. Mater. Chem.*, 2012, **22**, 7088.
- Handbook of Liquid Crystals*, ed. J. W. Goodby, C. Tschierske, P. Raynes, H. Gleeson, T. Kato and P. J. Collings, Wiley-VCH Verlag GmbH & Co. KGaA, Weinheim, Germany, 2014.
- T. Kato, T. Yasuda, Y. Kamikawa and M. Yoshio, *Chem. Commun.*, 2009, 729.
- J. Malthête, J. Jacques, N. H. Tinh and C. Destrade, *Nature*, 1982, **298**, 46–48.
- G. Scherowsky and X. H. Chen, *J. Mater. Chem.*, 1995, **5**, 417.
- R. J. Bushby and O. R. Lozman, *Curr. Opin. Colloid Interface Sci.*, 2002, **7**, 343–354.
- F. Vera, J. Luis Serrano and T. Sierra, *Chem. Soc. Rev.*, 2009, **38**, 781.
- T. Wöhrle, I. Wurzbach, J. Kirres, A. Kostidou, N. Kapernaum, J. Litterscheidt, J. C. Haenle, P. Staffeld, A. Baro, F. Giesselmann and S. Laschat, *Chem. Rev.*, 2016, **116**, 1139–1241.
- T. Metzroth, A. Hoffmann, R. Martin-Rapún, M. M. J. Smulders, K. Pieterse, A. R. A. Palmans, J. A. J. M. Vekemans, E. W. Meijer, H. W. Spiess and J. Gauss, *Chem. Sci.*, 2011, **2**, 69–76.
- D. Andrienko, V. Marcon and K. Kremer, *J. Chem. Phys.*, 2006, **125**, 124902.
- M. Yoneya, T. Makabe, A. Miyamoto, Y. Shimizu, Y. Miyake, H. Yoshida, A. Fujii and M. Ozaki, *Phys. Rev. E: Stat., Nonlinear, Soft Matter Phys.*, 2014, **89**, 062505.
- V. Marcon, D. W. Breiby, W. Pisula, J. Dahl, J. Kirkpatrick, S. Patwardhan, F. Grozema and D. Andrienko, *J. Am. Chem. Soc.*, 2009, **131**, 11426–11432.
- D. Chakrabarti and D. J. Wales, *Phys. Rev. Lett.*, 2008, **100**, 127801.
- X. Feng, V. Marcon, W. Pisula, M. R. Hansen, J. Kirkpatrick, F. Grozema, D. Andrienko, K. Kremer and K. Müllen, *Nat. Mater.*, 2009, **8**, 421–426.
- A. M. Giroud-Godquin and A. Rassat, *C. R. Seances Acad. Sci., Ser. 2*, 1982, **294**, 241–243.
- H. Zheng and T. M. Swager, *J. Am. Chem. Soc.*, 1994, **116**, 761–762.
- S. T. Trzaska, H.-F. Hsu and T. M. Swager, *J. Am. Chem. Soc.*, 1999, **121**, 4518–4519.
- J. Yoshida, H. Sato, A. Yamagishi and N. Hoshino, *J. Am. Chem. Soc.*, 2005, **127**, 8453–8456.
- J. Yoshida, H. Sato, N. Hoshino and A. Yamagishi, *J. Phys. Chem. B*, 2008, **112**, 9677–9683.
- G. Watanabe and J. Yoshida, *J. Phys. Chem. B*, 2016, **120**, 6858–6864.
- J. Yoshida, S. Tamura, K. Hoshino, H. Yuge, H. Sato, A. Yamazaki, S. Yoneda and G. Watanabe, *J. Phys. Chem. B*, 2018, **122**, 10615–10626.
- J. Yoshida, G. Watanabe, K. Kakizawa, Y. Kawabata and H. Yuge, *Inorg. Chem.*, 2013, **52**, 11042–11050.
- J.-G. Ha, J. Song, J.-K. Lee, B.-K. Cho and W.-C. Zin, *Chem. Commun.*, 2012, **48**, 3418.
- M. Hara, T. Orito, S. Nagano and T. Seki, *Chem. Commun.*, 2018, **54**, 1457–1460.
- W. Pisula, Ž. Tomović, C. Simpson, M. Kastler, T. Pakula and K. Müllen, *Chem. Mater.*, 2005, **17**, 4296–4303.
- M. Peterca, M. R. Imam, C.-H. Ahn, V. S. K. Balagurusamy, D. A. Wilson, B. M. Rosen and V. Percec, *J. Am. Chem. Soc.*, 2011, **133**, 2311–2328.
- J. Shu, D. Dudenko, M. Esmaili, J. H. Park, S. R. Puniredd, J. Y. Chang, D. W. Breiby, W. Pisula and M. R. Hansen, *J. Am. Chem. Soc.*, 2013, **135**, 11075–11086.
- M. L. Nguyen, J. Byun, S. Kim, J. W. Hyun, K. Hur, T. J. Shin and B. Cho, *Angew. Chem., Int. Ed.*, 2019, **58**, 2749–2753.
- N. V. Madhusudana, *Mol. Cryst. Liq. Cryst.*, 2004, **409**, 371–387.
- T. Nozawa, P. Brumby and K. Yasuoka, *Int. J. Mol. Sci.*, 2018, **19**, 2715.
- J. Yoshida, K. Tateyama and H. Yuge, *Dalton Trans.*, 2020, **49**, 2102–2111.
- M. Lehmann and M. Hügel, *Angew. Chem., Int. Ed.*, 2015, **54**, 4110–4114.
- K. Bader, T. Wöhrle, E. Öztürk, A. Baro and S. Laschat, *Soft Matter*, 2018, **14**, 6409–6414.
- M. Hügel, M. Dechant, N. Scheuring, T. Ghosh and M. Lehmann, *Chem. – Eur. J.*, 2019, **25**, 3352–3361.
- M. Lehmann, M. Dechant, M. Lambov and T. Ghosh, *Acc. Chem. Res.*, 2019, **52**, 1653–1664.